We are IntechOpen, the world's leading publisher of Open Access books
Built by scientists, for scientists

6,900
Open access books available

186,000
International authors and editors

200M
Downloads

154
Countries delivered to

Our authors are among the

TOP 1%
most cited scientists

12.2%
Contributors from top 500 universities

CLARIVATE ANALYTICS
BOOK CITATION INDEX
INDEXED

WEB OF SCIENCE™

Selection of our books indexed in the Book Citation Index
in Web of Science™ Core Collection (BKCI)

Interested in publishing with us?
Contact book.department@intechopen.com

Numbers displayed above are based on latest data collected.
For more information visit www.intechopen.com

Speckle Interferometry for Displacement Measurement and Hybrid Stress Analysis

Tae Hyun Baek[1] and Myung Soo Kim[2]
[1]School of Mechanical and Automotive Engineering, Kunsan National University,
[2]Department of Electronic Engineering, Kunsan National University,
Daehangno, Gunsan City,
Jeonbuk,
The Republic of Korea

1. Introduction

1.1 Application of ESPI to measurement of out-of-plane displacement in a spot welded canti-levered plate

Laser speckle interferometry can be used to detect the locations of stress concentration of an object and deformation over a whole area to be measured through the shape information in fringe patterns (Cloud, 1998; Petzing & Tyrer, 1998). ESPI can obtain interferometric fringes by a subtraction process ($I = |I_{before} - I_{after}|$) of the image data. Small displacement can be measured from such interferometric fringes corresponding to the order of the laser wavelength.

Several researches about in-plane displacement and vibration properties analyzed by ESPI have been reported and the application of ESPI is increasing (Rastogi, 2001). In this paper, the out-of-plane displacements of a partially spot welded canti-levered plate and of a normal canti-levered plate are measured and compared by application of 4-step phase shifting method to the analysis of fringe patterns in ESPI (Baek et al., 2002).

1.2 Optics of ESPI

1.2.1 ESPI for measurement of out-of-plane displacement

Figure 1-1 shows the arrangement of the ESPI optical system for measuring out-of-plane displacement. The interferometric fringe patterns caused by phase differences between the specimen and the reference plane with a PZT (piezoelectric transducer) must be analyzed because the interferometric fringe patterns contain information about out-of-plane displacement of the specimen. The phase difference is made by an optical path difference. The out-of-plane displacement, w, caused by the optical path difference is as follows:

$$w = \frac{\lambda}{4\pi}\phi \qquad (1\text{-}1)$$

In Eq. (1-1), w is z-directional (out-of-plane) displacement, λ is the wavelength of the laser, and ϕ represents the phase difference between before and after out-of-plane displacement.
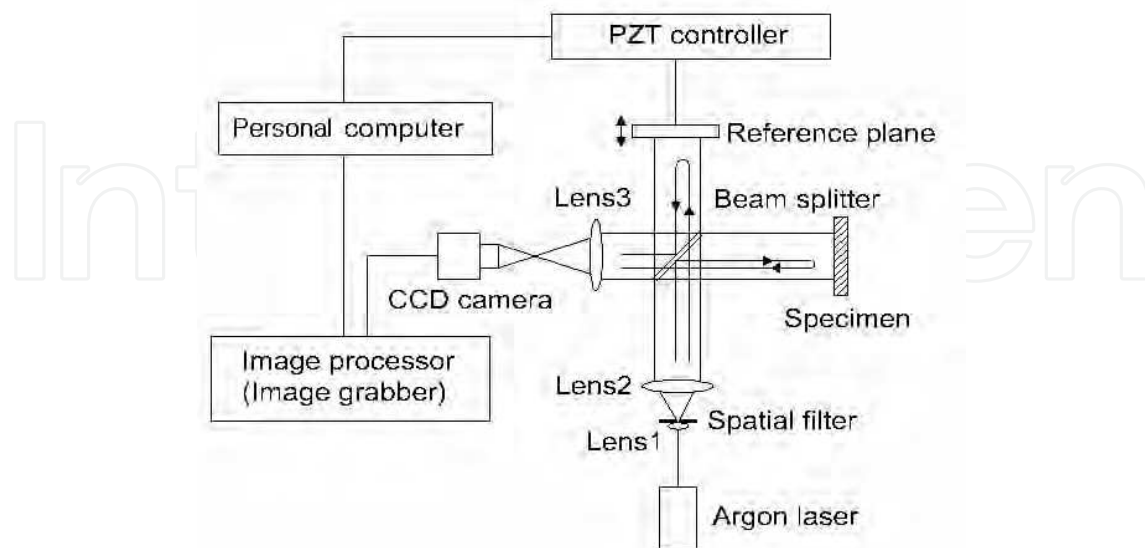

Fig. 1-1. Block diagram of ESPI optical system for measuring out-of-plane displacement.

1.2.2 4-step phase shifting method in ESPI

The 4-step phase shifting method used in this paper is employed to move the reference plane with the PZT by $\pi/2$ radians in each step and to obtain four fringe patterns with relative phase difference. The phase map is obtained from the four fringe patterns using the arc tangent function. The light intensity of the fringe pattern in ESPI, I_i, is expressed as follows:

$$I_i = I_0 \left\{ 1 + m(x, y) \cos[\phi(x, y) + \alpha] \right\} \tag{1-2}$$

In the above equation, $I_i(x, y)$ is the measured light intensity, I_0 is the average intensity, $m(x, y)$ is the contrast, $\phi(x, y)$ is the phase difference, and α is the phase introduced by PZT. The phase map, where the magnitude and sign of displacement can be known, can be obtained as follow.

$$\phi(x, y) = \tan^{-1} \left[\frac{I_4 - I_2}{I_1 - I_3} \right] \tag{1-3}$$

In Eq. (1-3), I_1, I_2, I_3 and I_4 are the light intensities at $\alpha = 0$, $\pi/2$, π, $3\pi/2$ radians, respectively. Eq. (1-3) uses the four fringe patterns with different phases, so that this method is called the 4-step phase shifting method. The phase map obtained by this method has the phase between $-\pi$ radians and $+\pi$ radians due to the property of the arc tangent function. Thus, the phase map has the discontinuous phase at every 2π radians, but this discontinuity can be eliminated by use of the phase unwrapping process and the continuous displacement of the specimen can be obtained (Ghiglia & Pritt, 1998).

The speckle pattern contains lots of noise and the noise must be filtered out before the phase unwrapping process. The Gaussian blur process in a commercial image processing software package (Adobe Photoshop, Version 5.5) is used to eliminate the speckle noise.

1.3 Experiment

1.3.1 Specimen and experimental set-up

The specimen used in this experiment is a 2 mm-thick canti-lever made of steel plate (E=200 GPa, $v = 0.3$). The shape and size of the specimen is shown in Fig. 1-2. Fig. 1-2 (a) is the normal canti-levered plate that is not spot-welded, and Fig. 1-2 (b) is the canti-levered plate that is spot-welded on the rear side.

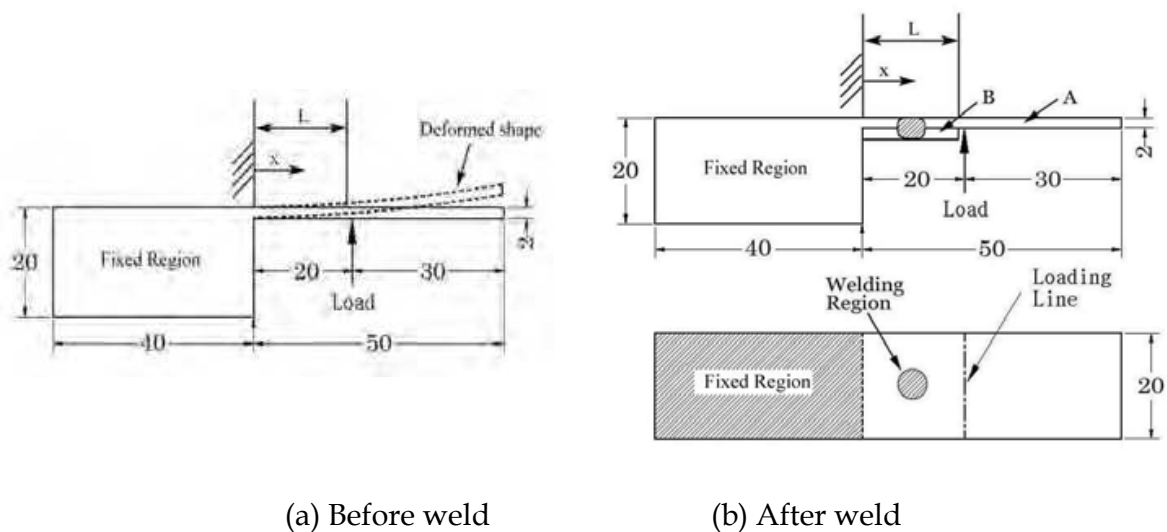
(a) Before weld   (b) After weld

Fig. 1-2. Dimensions of the specimen used for measurement of out-of-plane displacement. (a) Normal canti-levered plate, (b) Spot welded canti-levered plate.

Figure 1-3 shows the alignment of the optical components in which the optical set-up for Twyman-Green interferometry is used to measure the out-of-plane displacement. The phase shifting method is used to advance the precision degree of the speckle pattern in the measurement of out-of-plane displacement, and the phase shifting is performed by the PZT that is controlled with a personal computer.

The expression for the deflection curve for a canti-lever beam subjected to a concentrated load P, as shown in Fig. 1-2 (a), is

$$\delta = \frac{P}{6EI}\left(x^3 - 3Lx^2\right) \qquad (1\text{-}4)$$

In Eq. (1-4), E is the Young's elastic modulus, I is the moment of inertia, L is the distance from the fixed support to the loading point, and x is the distance from the fixed support to any arbitrary point.

Fig. 1-3 Optical systems for ESPI measurement of out-of-plane displacement.

1.3.2 Results of experiment

Figure 1-4 shows the speckle fringe patterns of a normal canti-lever at difference phases for $\alpha = 0,\ \pi/2,\ \pi,\ 3\pi/2$. Figure 1-5 shows the speckle fringe patterns of a spot welded canti-levered plate at difference phases for $\alpha = 0,\ \pi/2,\ \pi,\ 3\pi/2$. Those fringe patterns are obtained through a subtraction of before-displacement and after-displacement results of a specimen. The different phases in Figs. 1-4 and 1-5 are created by the PZT which controls the phases of fringe pattern by $\alpha = 0,\ \pi/2,\ \pi,\ 3\pi/2$, as mentioned before.

As seen in Figs. 1-4 and 1-5, the change of fringe patterns is shown near the welded area of the spot welded specimen. To eliminate the noise of the high frequency component in the speckle, the Gaussian blur process is applied to the original image obtained in the experiment. Figures 1-6 (a) and (b) are the original image and the Gaussian blurred image, respectively. When the Gaussian blurred image is compared with the original image in Fig. 1-6, it is clear that the high frequency noise is eliminated.

Figure 1-7 shows the light intensities along the line A-A in Fig. 1-6 (a) and (b). There is no doubt that the high frequency noise is eliminated in the Gaussian blurred image. Figure 1-8 is the phase map calculated by Eq. (1-3) in which four Gaussian blurred images are used.
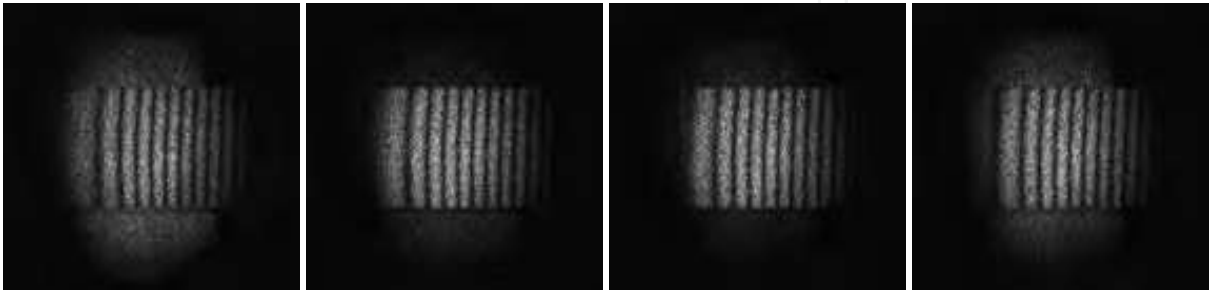

Fig. 1-4. Speckle fringe patterns of a normal canti-levered plate at difference phases for $\alpha = 0,\ \pi/2,\ \pi,\ 3\pi/2$ radians.
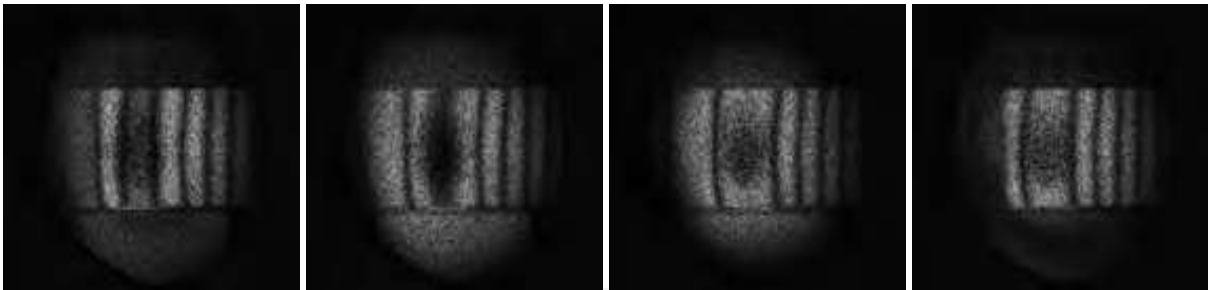
Fig. 1-5. Speckle fringe patterns of a spot welded canti-levered plate at difference phases for $\alpha = 0, \pi/2, \pi, 3\pi/2$ radians.
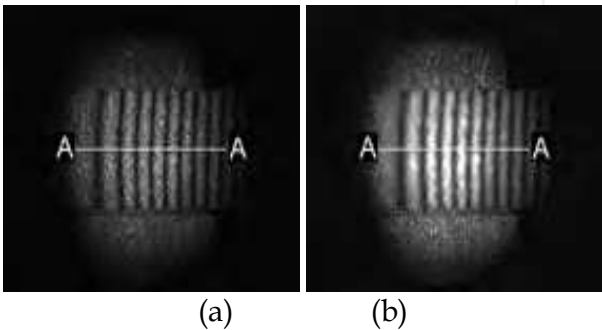

Fig. 1-6. (a) Original image and (b) Gaussian blurred image obtained from Fig. 1-4.
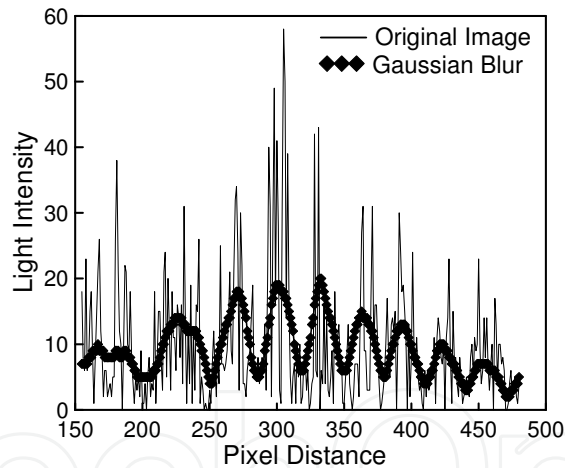

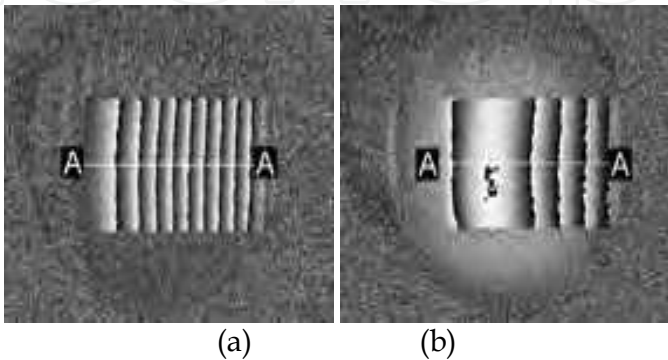Fig. 1-7. Comparison of light intensity along line A-A of Figs. 1-6 (a) and (b).

Fig. 1-8. Wrapped phase images of (a) normal and (b) spot welded canti-lever plate.
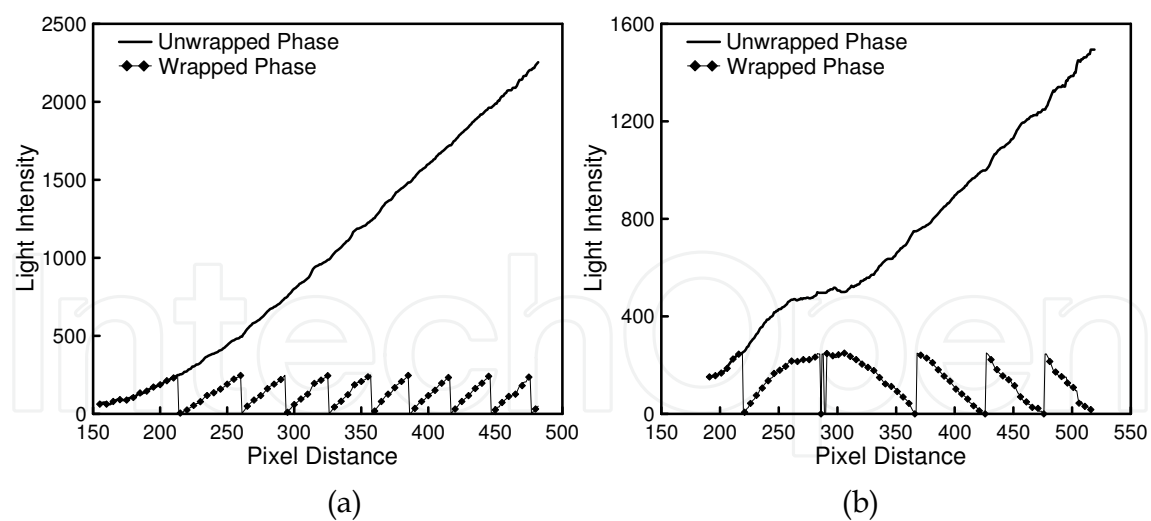
Fig. 1-9. (a) Wrapped and unwrapped phase distributions along line A-A of Fig. 1-8 (a) and along line A-A of Fig. 1-8 (b).

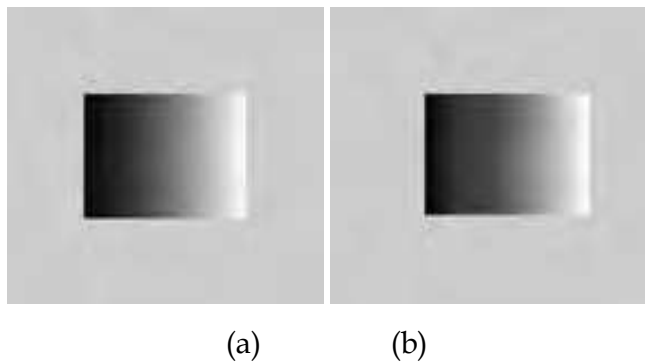   (a)   (b)

Fig. 1-10. Unwrapped phase maps of Fig. 1-8 (a) and (b).

When Figs. 1-8 (a) and (b) are compared, the phase map of the normal canti-levered plate is uniform, but that of the spot welded canti-levered plate shows a phase reversal at the welded area. Figure 1-9 (a) shows wrapped and unwrapped phase distributions along line A-A of Fig. 1-8 (a) of the normal canti-levered plate. Figure 1-9 (b) shows wrapped and unwrapped phase distributions along line A-A of Fig. 1-8 (b) of the spot welded canti-levered plate. Figure 1-10 (a) and (b) are the unwrapped phase maps of Fig. 1-8 (a) and (b). Figure 1-11 is 3-D view of the unwrapped phase image of Fig. 1-10. It is clearly seen in Figs. 1-11 (a) and (b) that continuous displacement occurred in the normal canti-levered plate but the displacement at the spot welded area was hump-shaped in the spot welded canti-levered plate.

Figure 1-12 (a) shows the displacement distribution obtained from the theory and from the phase shifting method along line A-A of Fig. 1-8. It shows that the result of ESPI is almost the same as that of the theoretical calculation for the normal canti-levered plate which is not spot welded. The maximum error of $0.076 \, \mu m$ occurs at approximately 7.9 mm from the fixed area of the canti-levered plate. However, in general, the measured displacement by the ESPI experiment is quite close to the theoretically expected displacement. Thus, it is proved that the physical out-of-plane displacement can be directly measured by the ESPI method.
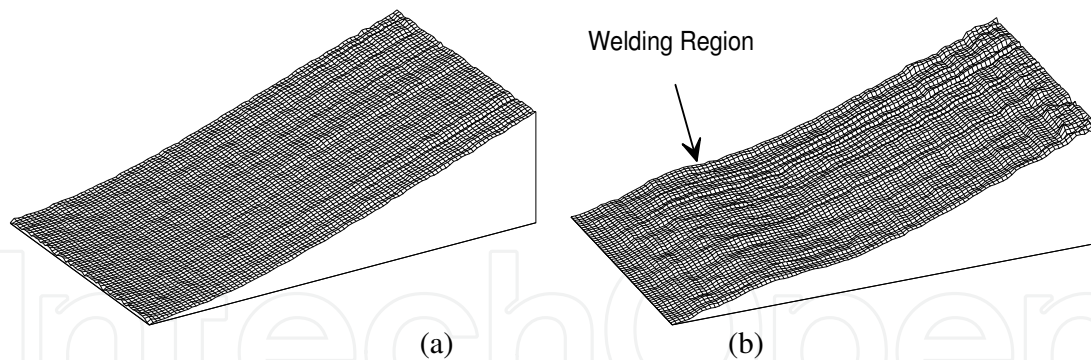
Fig. 1-11. 3-D view of unwrapped phase image of (a) Fig. 11(a) and (b) Fig. 11(b).
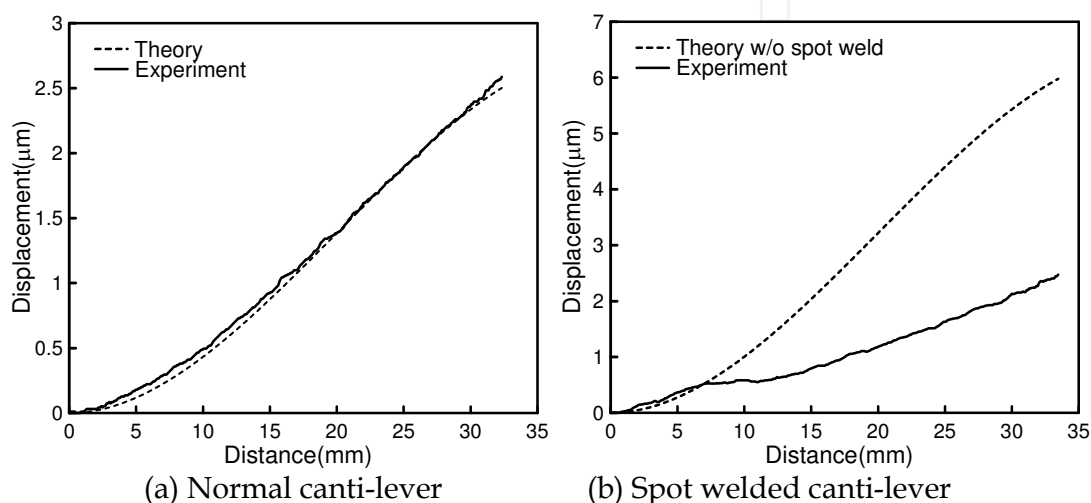

Fig. 1-12. Displacement distribution obtained from theory and from the phase shifting method along line A-A of Fig. 1-8 (a) and (b).

Figure 1-12 (b) shows the displacement distribution obtained from the spot welded canti-levered plate. The displacements, 0.582 μm , 1.183 μm , 2.134 μm , are measured at 10 mm, 20 mm, 30 mm from the fixed area of the spot welded canti-levered plate, respectively.

As a reference, the other displacements, 1.006 μm , 3.219 μm , 5.432 μm , are estimated at 10mm, 20mm, 30mm from the fixed area of the normal canti-levered plate. Therefore, the displacement for the same load decreases as the canti-levered plate is reinforced by spot-welding, and the spot welded area that is not visible can be easily detected by use of speckle interferometry.

1.4 Conclusions and discussions

The 4-step phase shifting method applied to an ESPI experiment has been used for the measurement of out-of-plane displacement in the normal canti-levered plate and the spot welded canti-levered plate. The measured displacement of the normal canti-levered plate agreed to the theoretical value within 0.076 μm . That is, it is proved that the physical out-of-plane displacement can be directly measured and precise measurement with a nanometer resolution is possible. Also, a welded area that is not visible from the surface can be detected and a small out-of-plane displacement in the welded area can be measured. The distribution

of displacement shows a slight non-linearity in the period of fringe, and therefore, further work is necessary for more precise measurement. Also, noise due to speckle has to be eliminated before the phase shifting method is applied. The Gaussian blur process is used to eliminate the noise in this work.

2. Measurement for in-plane displacement of tensile plates with through-thickness circular hole and partly through-thickness circular hole by use of speckle interferometry

2.1 Introduction

Speckle interferometry is an optical technique to measure displacement of a specimen by a coherent light from a laser. There are several phase extraction methods in speckle interferometry to measure the displacement, and phase shifting method (PSM) is one of the methods (Creath, 1988). In PSM, a known phase produced by piezoelectric transducer (PZT) is added into optical beam and resultant interference patterns are processed to get information about displacement of a specimen (Kim & Baek, 2006). In this paper, in-plane displacement of a steel plate with a partly through-thickness circular hole and a steel plate of a through-thickness circular hole is measured by simple optical system of speckle interferometry with PSM. Especially, the circular hole of steel plate with a partly through-thickness circular hole is not visible because the circular hole is cut on the rear side of the plate. This means that one cannot see any deformation or defect of the specimen.

2.2 Phase shifting method in speckle interferometry

Figure 2-1 is an optical system to measure in-plane displacement of specimens by use of PSM in speckle interferometry. A specimen is placed in a loading device and tensile load is applied to the specimen by the loading device in order to make in-plane displacement on the specimen. When two optical beams from a laser illuminate a specimen in speckle interferometry as shown Fig. 2-1, the optical beams make interference fringe patterns. The interference fringe patterns, I_i, can be represented by Eq. (2-1).

$$I_i = I_0 + I_c \cos\left[\phi(x, y) + \alpha_i\right] \tag{2-1}$$

where I_0 is the average intensity of fringe pattern and I_c is the contrast of fringe pattern.

A known phase, α_i, is added into one of the optical beams through controlling PZT. $\phi(x, y)$ is the phase of fringe pattern caused by the in-plane displacement of a specimen which tensile load is applied to. When 0, $\pi/2$, π, and $3\pi/2$ radians are used for α_i, four fringe patterns are taken through CCD camera and stored in PC. When I_1, I_2, I_3, and I_4, represent the fringe patterns for the known phases of 0, $\pi/2$, π, and $3\pi/2$ radians, respectively, the phase, $\phi(x, y)$, is calculated by use of Eq. (2-2).

$$\phi(x, y) = \tan^{-1}\left[\frac{I_4 - I_2}{I_1 - I_3}\right] \tag{2-2}$$

$\phi(x, y)$ in Eq. (2-2) is so-called wrapped phase. Unwrapped phase $\phi_u(x, y)$ is obtained with unwrapping algorithm of the wrapped phase (Ghiglia & Pritt, 1998). Then, the in-plane displacement of specimen, u, is obtained from the phase $\phi_u(x, y)$ as follows (Rastogi, 2001) ;

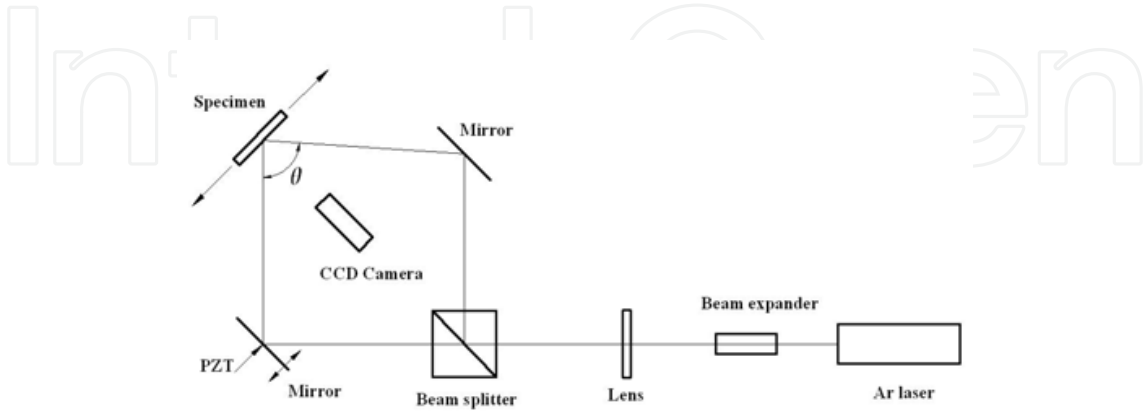$$u = \frac{\lambda}{4\pi \sin(\theta / 2)} \phi_u(x, y) \qquad (2\text{-}3)$$

Fig. 2-1. Schematic diagram of speckle interferometry with phase-shifting method for in-plane displacement measurement (θ is the angle between two incident lights onto the specimen).

2.3 Optical experiment

The specimens used in this experiment are a rectangular steel plate with a through-thickness circular hole at the center and a rectangular steel plate with a partly through-thickness circular hole at the center on rear side as in Fig. 2-2. Both of the rectangular steel plates have the same size that is 147 mm x 27.7 mm with thickness of 1.2 mm. The diameter of through-thickness circular hole is 12 mm. Also the diameter of partly through-thickness circular hole is 12 mm but it is uniformly cut by 0.8 mm on the rear side. Figure 2-3 is the picture of optical experiment system. Ar laser with wavelength of 515 nm is used in the optical experiment.
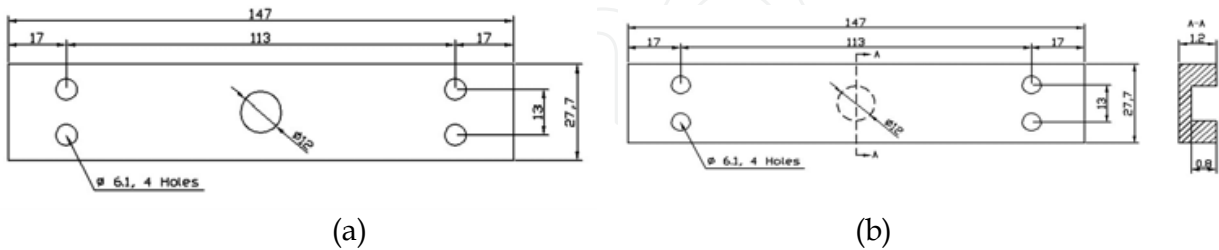

(a)   (b)

Fig. 2-2. Dimensions of specimens used in-plane displacement (unit : mm) (a) rectangular steel plate with through-thickness circular hole (b) rectangular steel plate with partly through-thickness circular hole.

At first, optical experiment is performed with the steel plate with through-thickness circular hole at the center. Four fringe patterns, I_1, I_2, I_3, and I_4, are taken in the experiment and they are stored in PC. However, the four fringe patterns have lots of speckle noises, so that

they are processed by use of an image processing algorithm. In this work, Gaussian blur algorithm that is available commercially in Adobe Photoshop is used to process the fringe patterns. The processed four fringe patterns are shown in Fig. 2-4. The same experimental procedures are used to get four fringe patterns for the steel plate with partly through-thickness circular hole at the center on rear side.

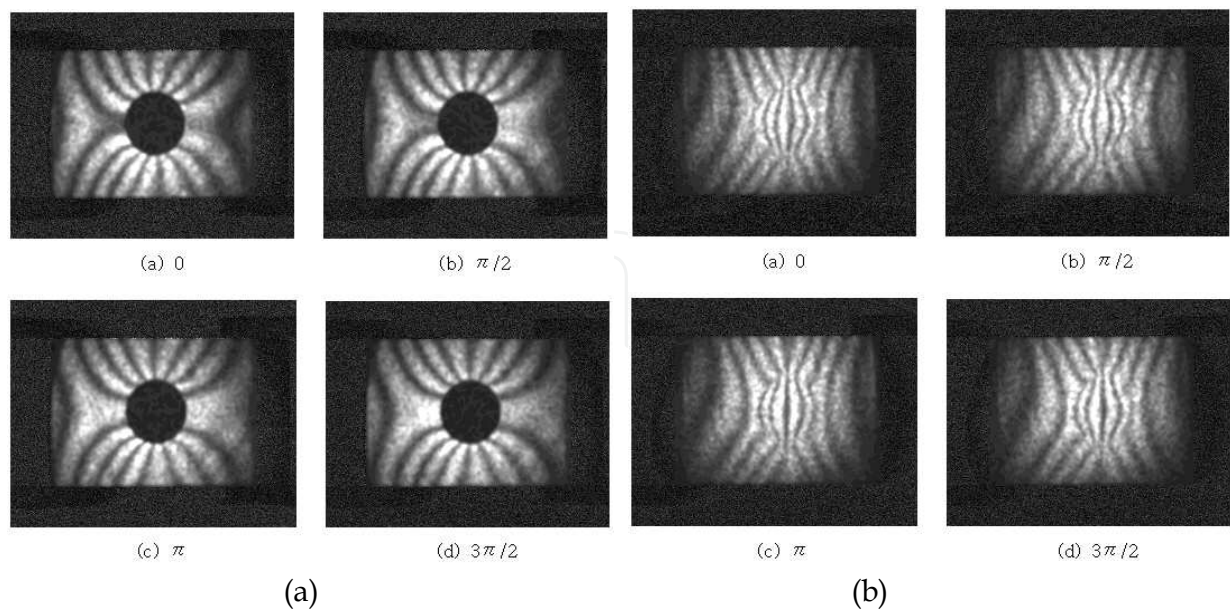Fig. 2-3. Optical setup for measurement of in-plane displacement.

Fig. 2-4. Fringe patterns of specimen : (a) Steel plate with a through-thickness circular hole processed by Gaussian Blur (b) Steel plate with a partly through-thickness circular hole processed by Gaussian Blur.
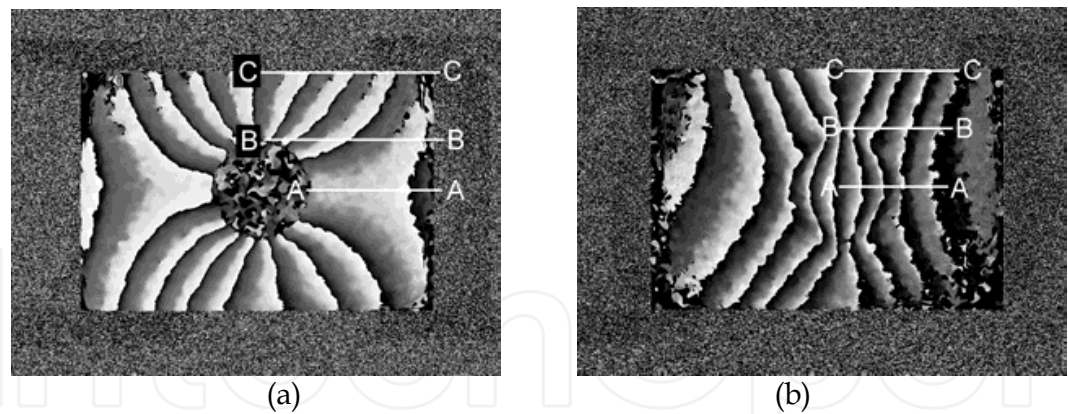
(a)   (b)

Fig. 2-5. Wrapped phase maps (a) steel plate with a through-thickness circular hole, (b) steel plate with a partly through-thickness circular hole.
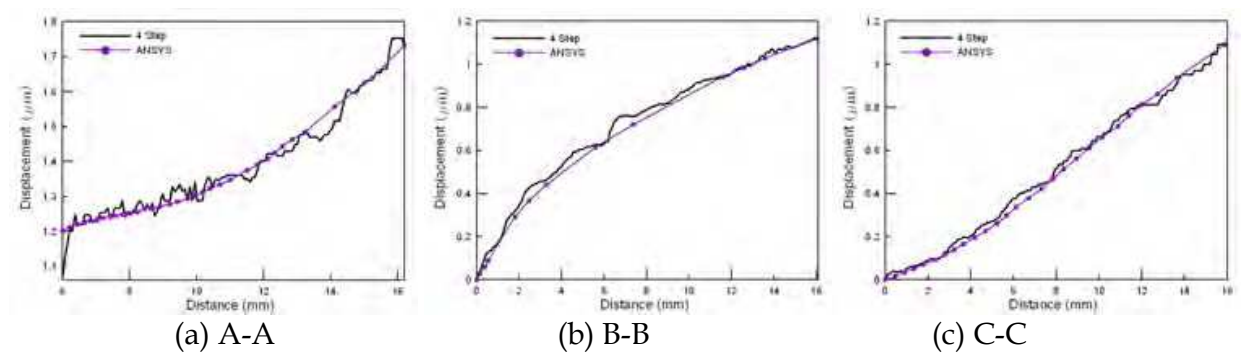

(a) A-A   (b) B-B   (c) C-C

Fig. 2-6. Displacement distribution along A-A, B-B, and C-C line of Fig. 2-5 (a).

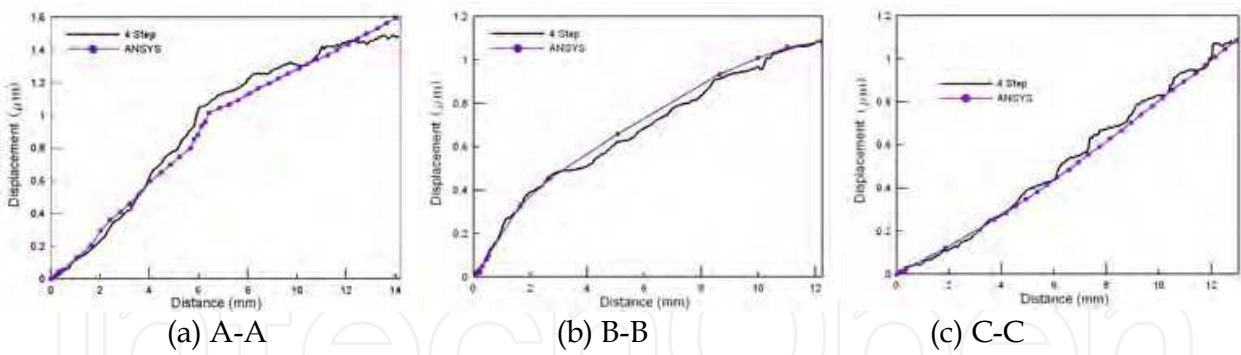(a) A-A   (b) B-B   (c) C-C

Fig. 2-7. Displacement distribution along A-A, B-B, and C-C line of Fig. 2-5 (b).

Using Eq. (2-2), the wrapped phases, $\phi(x, y)$, are obtained for the two specimens and shown in Fig. 2-5 (a) and (b). Quantitative data are acquired along the lines, A-A, B-B, and C-C in Fig. 2-5. The phases, $\phi(x, y)$, along the lines are unwrapped and the in-plane displacement of the specimens is plotted in Figs. 2-6 and 2-7 by use of Eq. (2-3).

For comparative purpose, the two specimens of Fig. 2-2 are analyzed by ANSYS. Figures 2-8 (a) and (b) are the models for ANSYS. The physical properties used for the analysis are the same as the physical properties of structural steel that are E=200 GPa and $v = 0.3$. The ANSYS discretization for the rectangular steel plate with a through-thickness circular hole at the center used 8 node quadrilateral elements. The ANSYS discretization for the rectangular

steel plate with a partly through-thickness circular hole at the center used 10 node tetrahedral elements.

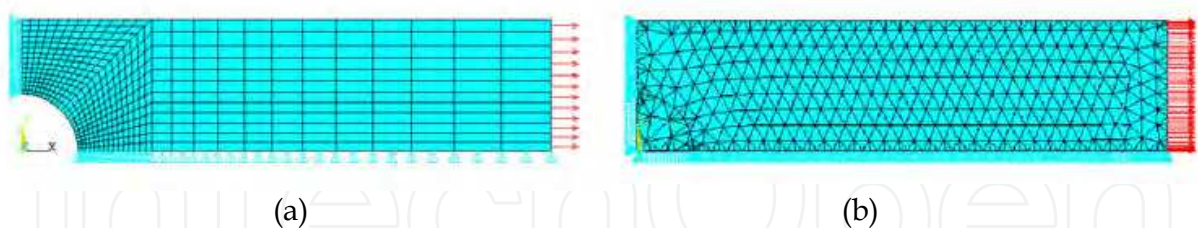(a)   (b)

Fig. 2-8. ANSYS discretization. (a) Steel plate with a circular hole in Fig. 2 (a). (b) Steel plate with partly through-thickness circular hole in Fig. 2 (b).

The results of the two specimens from ANYSYS are plotted also in Figs. 2-6 and 2-7. As shown in Figs. 2-6 and 2-7, the results of the optical experiments for speckle interferometry with 4-step phase shifting method agree with those of ANSYS.

2.4 Conclusions and discussions

In-plane displacements of two specimens are measured by simple optical system of speckle interferometry using 4-step phase shifting method; one is the rectangular steel plate with a through-thickness circular hole and the other is the rectangular steel plate with a partly through-thickness circular hole. The circular hole of the steel plate with a partly through-thickness circular hole is not visible because the circular hole is cut on the rear side of the plate, so that one cannot see any deformation or defect of the specimen. The fringe patterns acquired by optical experiment of speckle interferometry are processed by image processing algorithm of Gaussian blur in Adobe Photoshop and the in-plane displacements of the two specimens are obtained by the processed fringe patterns. Also the in-plane displacements of the two specimens are calculated by use of ANSYS.

The results of optical experiments are quite comparable to those of calculation with ANSYS. Based on the optical experiments, speckle interferometry can be applied to easily detect or measure defect or deformation in a specimen that is not visible.

3. A hybrid stress measurement using only x-displacements by Phase Shifting Method with Fourier Transform (PSM/FT) in laser speckle interferometry and least squares method

3.1 Introduction

Stress raisers have been one of the main concerns when it comes to design analysis. Due to the complexities associated with it, numerous and continuing investigation are done to develop techniques to accurately measure stress concentration around the geometric boundaries. Several methods can be found in the literature ranging from FEM, the use of photoelastic-data, hybrid method and other various numerical and experimental procedures (Lekhnitskii; Tsai & Cheron, 1968; Kobayshi, 1993; Dally & Riley, 1991; Pilkey's, 2008).

In this paper, we present stress concentration measurement method using only x-component displacement data of selected points along straight lines away from the

geometric discontinuity. In conjunction with our previous studies (Baek et al., 2000; Baek & Rowlands, 1999; Baek & Kim, 2005; Baek et al., 2006), the hybrid method employing the least-squares method integrated with Laurent series representation of the stress function was used to estimate reliable edge data around the circular hole in a tensile-loaded plate from a relatively few measured x-displacement data away from the boundary. Speckle interferometry has been explored and integrated with other methods for the optical measurement of in-plane and out-of-plane displacement in a material (Schwider, 1989; Steinzig & Takahashi, 2006). Different from the previous works, this study utilized considerably a few number of in-plane micro-scale x-displacement only measured by speckle interferometry using PSM/FT for hybrid stress analysis.

The present technique employs fairly general expressions for the stress functions, and traction-free conditions which are satisfied at the geometric discontinuity using conformal mapping and analytical continuation. The approach is illustrated using the x-displacement as input data obtained from phase-shifting method in speckle interferometry.

3.2 Theoretical background

3.2.1 Basic equations

In the absence of body forces and rigid body motion, the stresses and displacements under plane and rectilinear orthotropy can be written as (Gerhardt, 1984; Rhee & Rowlands, 2002).

$$
\begin{aligned}
u &= 2\,\mathrm{Re}\big[\,p_1\Phi(\zeta_1) + p_2\Psi(\zeta_2)\,\big] \\
v &= 2\,\mathrm{Re}\big[\,q_1\Phi(\zeta_1) + q_2\Psi(\zeta_2)\,\big].
\end{aligned}
\tag{3-1}
$$

The two complex stress functions $\Phi(\zeta_1)$ and $\Psi(\zeta_2)$ are related to each other by the conformal mapping and analytic continuation. For a traction-free physical boundary, the two functions within sub-region Ω of Fig. 3-1 can be written as Laurent expansions, respectively (Gerhardt, 1984; Baek & Rowlands, 2001)

$$
\Phi(\zeta_1) = \sum_{k=-m}^{m} \zeta_1^k \quad \text{and} \quad \Psi(\zeta_2) = \sum_{k=-m}^{m} \left(\overline{c_k} B \zeta_2^k + c_k C \zeta_2^k \right)
\tag{3-2}
$$

The coefficients of Eq. (3-2) are $c_k = a_k + i b_k$ where a_k and b_k are real numbers. In addition to satisfying the traction-free conditions on the hole boundary Γ, the stresses and displacements of Eqs. (3-1) and (3-2) associated with these stress functions $\Phi(\zeta_1)$ and $\Psi(\zeta_2)$ satisfy equilibrium and compatibility.
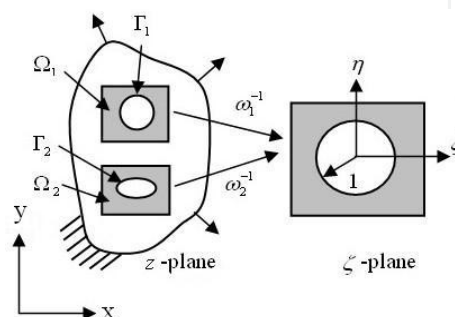

Fig. 3-1. Mapping of holes from the physical z-plane into the ζ-plane.

The primes denote differentiation with respect to the argument. Complex material parameters μ_l (l = 1, 2) are the two distinct roots of the characteristic Eq. (3-3) for an orthotropic material under plane stress (Lekhnitskii, Tsai & Cheron, 1968; Gerhardt, 1984)

$$S_{11}\mu^4 + (2S_{12} + S_{66})\mu^2 + S_{22} = 0 \tag{3-3}$$

where S_{ij} are the elastic compliances. The material properties p_l and q_l are defined as

$$
\begin{aligned}
p_1 &= S_{11}\mu_1^2 + S_{12}, \quad p_2 = S_{11}\mu_2^2 + S_{12} \\
q_1 &= S_{12}\mu_1 + \frac{S_{22}}{\mu_1}, \quad q_2 = S_{12}\mu_2 + \frac{S_{22}}{\mu_2}
\end{aligned} \tag{3-4}
$$

The inverse of the mapping function ω namely ω^{-1}, maps the geometry of interest from the physical z-plane into the ζ-plane ($\zeta_l = \xi + \mu_l \eta$). For orthotropic materials, the conformal transformation from the unit circle in the ζ-plane to the hole in the z-plane of radius R is shown in Fig. 3-1 and is given by

$$z_l = \omega_l(\zeta_l) = \frac{R}{2}\left[(1 - i\mu_l)\zeta_l + \frac{1 - i\mu_l}{\zeta_l}\right] \tag{3-5}$$

where $i = \sqrt{-1}$. The inverse of (3-5) is

$$\omega^{-1}(z_l) = \zeta_l = \frac{z_l \pm \sqrt{z_l^2 - R^2(1 + \mu_l^2)}}{R(1 - i\mu_l)} \tag{3-6}$$

The branch of the square root of Eq. (3-6) is chosen so that $|\zeta_l| \geq 1$ (l = 1, 2). Complex quantities B and C in Eq. (3-2) depend on material properties defined as

$$B = \frac{\bar{\mu}_2 - \bar{\mu}_1}{\mu_2 - \bar{\mu}_2}, \quad C = \frac{\bar{\mu}_2 - \mu_1}{\mu_2 - \bar{\mu}_2} \tag{3-7}$$

3.2.2 Least-squares method

Combining Eqs. (3-2), (3-3) and (3-5) gives the following expressions for the displacements through regions Ω_1 and Ω_2 of Fig. 3-1. In matrix form,

$$\{d\} = [U]\{c\} \tag{3-8}$$

where $\{u\} = \{u, v\}^{\mathrm{T}}$, and $\{c\} = \{a_k, b_k\}^{\mathrm{T}}$. $[U]$ is a rectangular coefficient matrix whose size depends on the number of terms k of the power series expansions of Eq. (3-1) and given by

$$U(1, j) = 2\,\mathrm{Re}\left\{p_1\zeta_1^k + p_2(C\zeta_2^k + B\zeta_2^{-k})\right\} \tag{3-9a}$$

$$U(2, j) = 2\,\mathrm{Re}\left\{q_1\zeta_1^k + q_2(C\zeta_2^k + B\zeta_2^{-k})\right\} \tag{3-9b}$$

In Eqs. (3-9a) and (3-9b), $j = 2(k + m) + 1$ if $k < 0$ and $j = 2(k + m) - 1$ if $k > 0$.

Knowing $\{d\}$ at various locations in Eq. (3-8) allows the best values of unknown coefficients $\{c\}$ in a least square sense (Sanford, 1980). For n measured x-displacements and m terms, the coefficients $\{c\}$ of Eqs. (3-8) were obtained from Eq. (3-10) by the least squares method expressed as

$$\{c\}_{m+1} = \left([U]^T_{[(m+1)\times 2n]} [U]_{[2n\times(m+1)]} \right)^{-1} [U]^T_{[(m+1)\times 2n]} \{d\}_{(2n\times 1)} \tag{3-10}$$

3.2.3 In-plane displacement by speckle interferometry

In speckle interferometry using phase-shifting method with Fourier transformation (PSM/FT) (Morimoto & Fujisawa, 1994), interference fringe pattern is obtained by subtracting the pattern from the pre-loading and post-loading conditions of the specimen. The intensity of the fringe pattern is calculated as

$$I(x, y : \alpha) = A(x, y)\cos[\phi(x, y) - \alpha] + B(x, y) \tag{3-11}$$

where $A(x,y)$ is the amplitude of the brightness in the pattern and $B(x,y)$ is the average brightness. Piezoelectric transducer (PZT) can control an optical path length. α is the known phase which is added into one of the two optical beams by controlling the PZT. The known phase α covers the region from 0 to 2π radians at equal intervals. $\phi(x,y)$ is the phase of fringe pattern caused by the in-plane displacement of a specimen.

A phase-shifting method using Fourier transform had been well-developed for the measurement of in-plane displacement by speckle interferometry (Morimoto & Fujisawa, 1994; Kim et al., 2005). The phase ϕ can be calculated as

$$\phi(x, y) = -\tan^{-1}\left(\frac{\text{Im}\left[F_\alpha(x, y : \omega_0) \right]}{\text{Re}\left[F_\alpha(x, y : \omega_0) \right]} \right) \tag{3-12}$$

where

$$F_\alpha(x, y : \omega_0) = \int_{-\pi}^{\pi} \left[A\cos(\phi(x, y) - \alpha) + B \right] e^{-j\alpha} d\alpha = \pi A e^{-j\phi(x, y)} \tag{3-13}$$

is the α-directional Fourier transform of Eq. (3-11). In Eqs. (3-12) and (3-13), ω_0 is a fundamental frequency. Using the calculated phase, ϕ, the displacement of a specimen can be obtained.

3.3 Optical experiments

Speckle interferometry experiment was performed with setup as shown in Fig. 3-2 to acquire the needed data. In Fig. 3-2, LA is a laser, PA is a pin-hole assembly, CL is a collimating lens, BS is a non-polarizing beam splitter, MR1 and MR2 are mirrors. SL is a specimen installed in a tensile loading device, CCD is a CCD camera, and PC is a personal computer. PC controls the movement of PZT through the control board CNT (Kim et al., 2005).

Figure 3-3 shows the steel plate specimen (E=200 GPa, $\nu = 0.3$) which was subjected to tensile load during the procedure. The test specimen of Fig. 3 had been used for experiment for the development and application of phase-shifting method in speckle interferometry. The accuracy and reliability of the said in-plane displacement measuring method had been established (Baek et al., 2008). For this reason, it is a useful tool for the hybrid stress analysis presented herein (Baek & Rowlands, 1999; Baek & Rowlands, 2001). In this study, phase-shifting method using Fourier transform was utilized.

Fig. 3-2. Schematic diagram of speckle interferometry experiment for x-displacement data acquisition.

Figure 3-4 shows the picture of optical experiment system for speckle interferometry by PSM/FT. The in-plane x-displacement of the specimen, u, along the longitudinal direction is obtained through

$$u = \frac{\lambda}{4\pi \sin \theta} \phi_u \qquad (3-14)$$

where u is the longitudinal displacement, λ is the wavelength of light from a laser and ϕ_u is the phase obtained from longitudinal displacement.
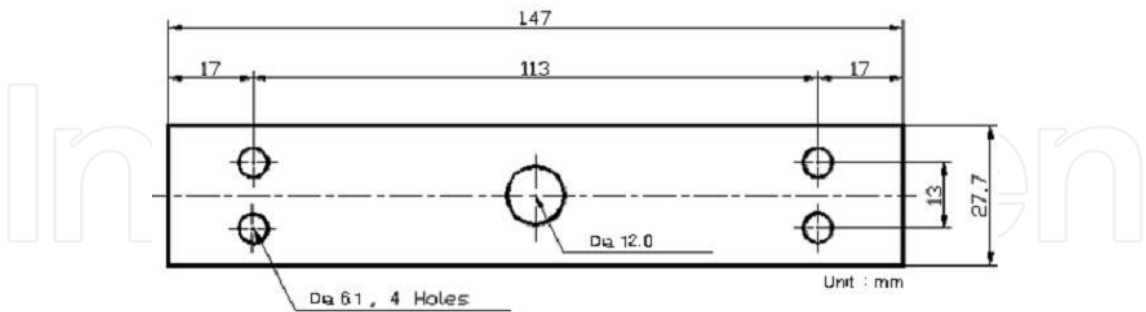

Fig. 3-3. Finite-width uni-axially tensile-loaded steel plate.

The laser used in the experiment is He-Ne laser and λ is 633 nm. The angle between incident light and vertical line to the specimen, θ as shown in Fig. 3-2, is around $26°$. The specimen is installed in a loading device that applies tensile load to the specimen in order to make in-plane displacement. Fringe patterns of $I(x, y : \alpha)$ in Eq. (3-11) are taken through CCD camera in Fig. 3-2. The fringe patterns consist of 32 patterns which are sequentially phase-shifted by PZT stage and are saved in PC. Phase shifting at each step is $\pi/16$ radian.

Size of each fringe pattern is 640 x 480 with 8 bits brightness. 16 fringe patterns out of the 32 fringe patterns are shown as examples at every interval of $\pi/8$ radian for the rectangular steel plate containing a hole in Fig. 3-5 (Kim et al., 2005).
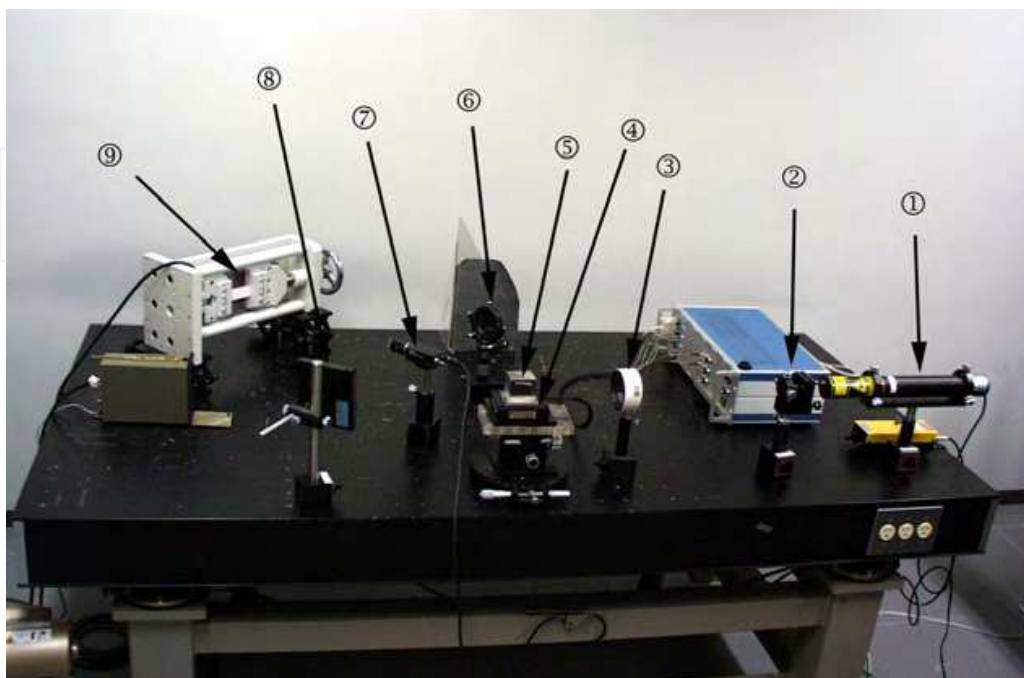

Fig. 3-4. Picture of optical experiment system for speckle interferometry by PSM/FT. (① He-Ne CW laser, ②pin-hole assembly, ③ collimating lens, ④ PZT control stage, ⑤ beam splitter, ⑥ mirror, ⑦ CCD camera, ⑧ mirror, ⑨ specimen in loading device).

The accuracy of the least-squares method for calculating displacement components $\{u,v\}^T$ as presented in the preceding section was related with the input data acquired through experiment by phase-shifting method in speckle interferometry (Baek & Rudolphi, 2010).

Percent errors for each data was calculated and shown in Table 3-1. As can be observed, the level of precision of the hybrid method is too close with the original input data as indicated by the % Errors. Thus, the method is significantly accurate and reliable for calculating such parameter.

The simplicity of the test specimen being isotropic, containing symmetrically-shaped discontinuity facilitates the ease of reliable verification. Finite element anlysis was done to establish a benchmark for comparison purposes. Figure 3-7 shows the ABAQUS discretization of the quarter steel plate. In the vicinity of the circular hole, the ABAQUS model of Fig. 3-7 utilizes elements on the edge of the hole as small as 1.5° by $0.013r$, where r is the radius of the circular hole. Tangential stress around the quarter hole was determined and compared as shown in Fig. 3-8. Different values of m term in the complex stress functions was tested to see its effect, it came out that at point of high stress concentration ($\theta = 90^{\circ}$ in Fig. 3-8). Well-comparable results were attained at decreasing value of m with the best value equal to 1 – accurate by less than one percent error. Figure 3-9 reveals the preceding observation and shows normalized tangential stress at the edge of the quarter hole in a steel plate with $m = 1$ in the complex stress function.
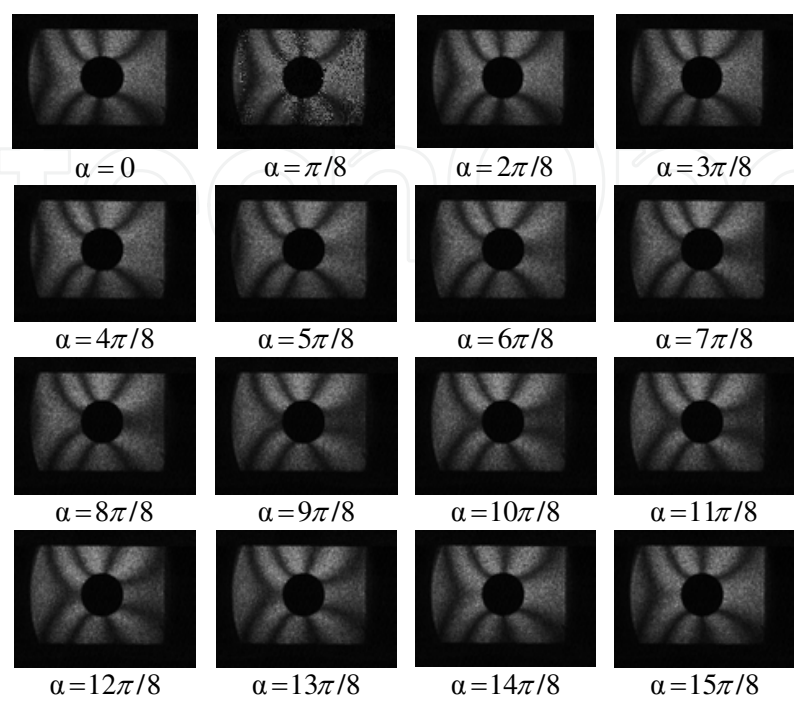
$\alpha = 0$ $\alpha = \pi/8$ $\alpha = 2\pi/8$ $\alpha = 3\pi/8$

$\alpha = 4\pi/8$ $\alpha = 5\pi/8$ $\alpha = 6\pi/8$ $\alpha = 7\pi/8$

$\alpha = 8\pi/8$ $\alpha = 9\pi/8$ $\alpha = 10\pi/8$ $\alpha = 11\pi/8$

$\alpha = 12\pi/8$ $\alpha = 13\pi/8$ $\alpha = 14\pi/8$ $\alpha = 15\pi/8$

Fig. 3-5. 16 fringe patterns of rectangular steel plate containing a circular hole at every interval of $\alpha = \pi/8$ radian.
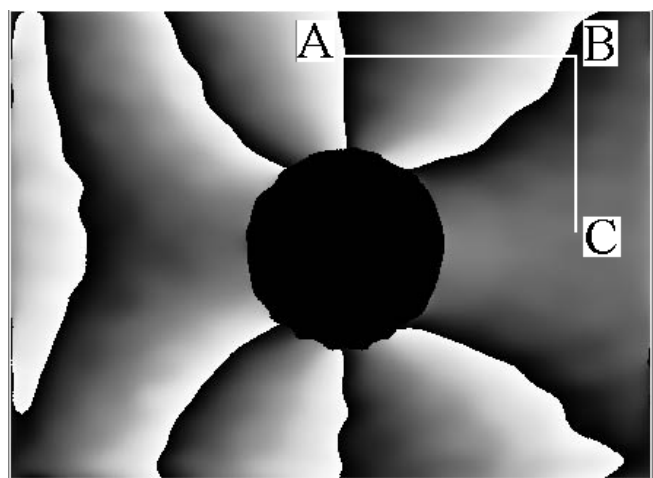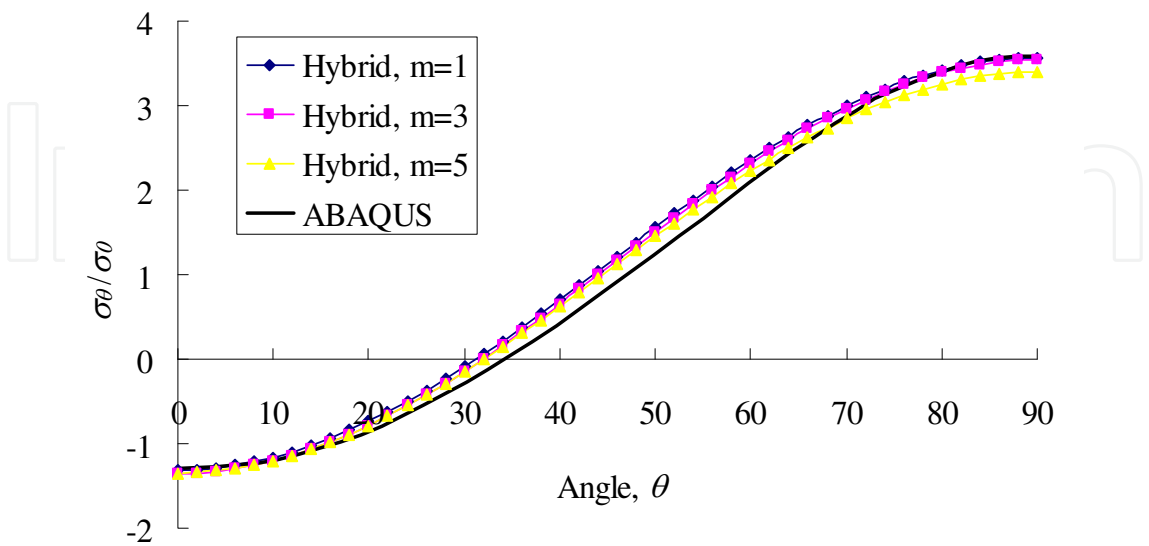

Fig. 3-6. Wrapped phase of steel plate with circular hole. Lines AB and BC are x-displacement extraction regions.

Data Point	Input: x-disp. (μm)	Calculated: x-disp. (μm)	% Error*
1	0	0	-
2	2.6032	2.5791	-0.926
3	2.8628	2.8397	-0.807
4	4.3754	4.3678	-0.174
5	5.5334	5.5499	0.298
6	6.8069	6.8555	0.714
7	7.3259	7.3421	0.221
8	7.8783	7.8483	-0.381
9	8.0719	8.0536	-0.227

*Note: $\%\text{Error} = \dfrac{\text{Calculated} - \text{Input}}{\text{Input}} \times 100(\%)$

Table 3-1. Comparison between input and calculated x-displacement for different values of $m = 1$ of the complex stress functions.

Fig. 3-7. ABAQUS discretization of the quarter steel plate (t = 1.15mm).

Fig. 3-8. Normalized tangential stress at the edge of the quarter hole in a steel plate with different values of m term in the complex stress function.
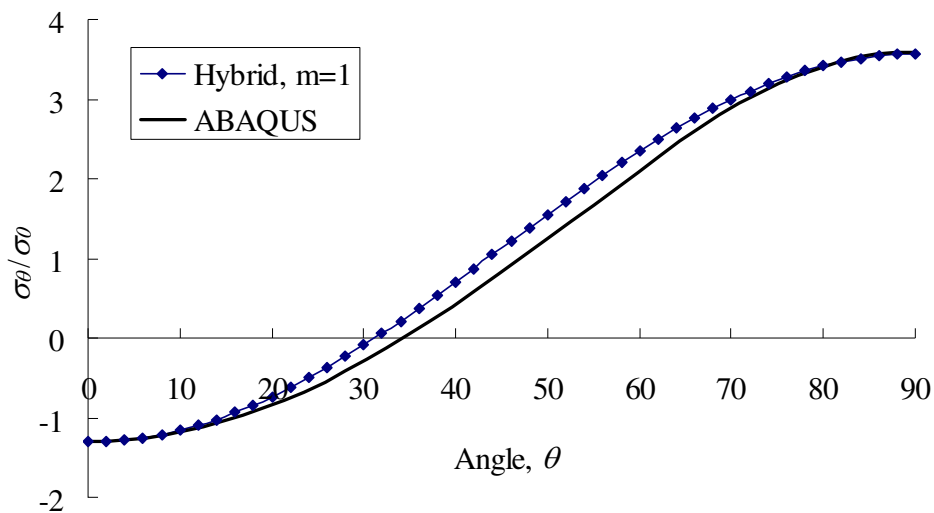
Fig. 3-9. Normalized tangential stress at the edge of the quarter hole in a steel plate with $m = 1$ in the complex stress function.

3.4 Conclusions and discussions

A reliable hybrid method for characterizing stress around the circular hole in a tensile-loaded steel plate is presented. The method utilized only few micro-scale x-displacement data measured by a well-established optical technique, speckle interferometry, in conjunction with phase shifting method using Fourier transform to calculate stress components and eventually stress concentration at $\theta = 90^\circ$. The use of few input data may reduce experiment time and relatively increase data processing speed.

Different values of m term in the complex stress functions were tested to see its effect. In the comparison between input x-displacement data and calculated data the hybrid method is effective with an error below 1% in all values of *m*. On the other hand, it came out that at point of high stress concentration ($\theta = 90^\circ$), well-comparable results were attained at decreasing value of *m*. The best value of m is consistently known to be equal to 1 of which results are accurate by less than one percent error. Results showed that the method is accurate and reliable as compared with the widely-used FEM software, ABAQUS.
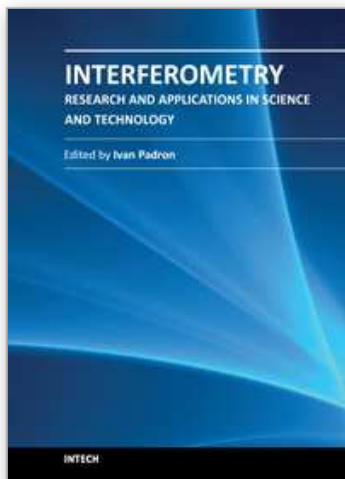
4. Acknowledgement

5. References

Cloud, G. (1998). *Optical Methods of Engineering Analysis*, Cambridge University Press, ISBN 978-0521636421, Cambridge, United Kingdom

Petzing, J. & Tyrer, J. (1998). Recent Developments and Applications in Electronic Speckle Pattern Interferometry, *Journal of Strain Analysis*, Vol.33, No.2, pp. 153-169, ISSN 0309-3247

Rastogi, P. (Editor) (2001). *Digital Speckle Pattern Interferometry and Related Techniques,* John Wiley and Sons, Ltd., ISBN 978-0471490524, New York, USA

Baek, T.; Kim, M., Na, E. & Koh, S. (2003). Application of ESPI to Measurement of Out-of-plane Displacement in a Spot Welded Canti-levered Plate, *International Journal of the Korean Society of Precision Engineering*, Vol.4, No.5, pp. 41-46

Ghiglia, D. & Pritt, M. (1998). *Two-Dimensional Phase Unwrapping*, John Wiley & Sons, Inc., ISBN 978-0471249351, New York, USA

Creath, K. (1988). Phase-measurement interferometry techniques, *Progress in Optics*, Vol.26, pp. 349-393, ISSN 0079-6638

Kim, M. & Baek, T. (2006). Measurement for in-plane displacement of tensile plates with partly through-thickness circular hole and through-thickness circular hole by use of speckle interferometry, *Key Engineering Materials*, Vols.321-323, pp. 77-80, ISSN 1162-9795

Lekhnitskii, S.; Tsai, S. & Cheron, T. (1968). *Anisotropic Plates*, Gordon and Breach

Kobayshi, A. (Editor) (1993). *Handbook on Experimental Mechanics,* 2nd Revised Edition, Society for Experimental Mechanics, VCH Publishers, Inc., ISBN 978-1560816409,

Dally, J. & Riley, W. (1991). Experimental Stress Analysis, 3rd Edition, McGraw-Hill, Inc., New York, USA

Pilkey, W. & Pilkey, D. (2008). *Peterson's Stress Concentration Factors*, John Wiley & Sons, Inc., ISBN 978-0470048245, New Jersey, USA

Baek, T.; Kim, M., Rhee, J. & Rowlands, R. (2000). Hybrid Stress Analysis of Perforated Tensile Plates using Multiplied and Sharpened Photoelastic Data and Complex-Variable Techniques, *JSME International Journal, Series A: Solid Mechanics and Material Engineering*, Vol.43, No.4, pp. 327-333, ISSN 0914-8809

Baek, T. & Rowlands, R. (1999). Experimental Determination of Stress Concentrations in Orthotropic Composites, *Journal of Strain Analysis*, Vol.34, No.2, pp. 69-81, ISSN 0309-3247

Baek, T. & Kim, M. (2005). Computer Simulation of Photoelastic Fringe Patterns for Stress Analysis, *Lecture Notes in Computer Science*, Vol.3398, pp. 214-221, ISSN 0302-9743

Baek, T. Koh, S. & Park, T. (2006). An Improved Hybrid Full-field Stress Analysis of Circularly Perforated Plate by Photoelasticity and Finite Element Analysis, *Key Engineering Materials*, Vol.326-328, pp. 1209-1212, ISSN 1162-9795

Schwider, J. (1989). Phase shifting Interferometry: reference phase error reduction, Applied Optics, Vol.28, Issue 18, pp. 3889-3892

Steinzig, M. & Takahashi, T. (2006). Residual Stress Measurement Using the Hole Drilling Method and Laser Speckle Interferometry, Part IV: Measurement Accuracy, Experimental Techniques, Vol. 27, Issue 6, pp. 59-63, ISSN 0732-8818

Gerhardt, T. (1984). A Hybrid/Finite Element Approach for Stress Analysis of Notched Anisotropic Material, *ASME Journal of Applied Mechanics*, Vol.51, No.4, pp. 804-810

Rhee, J. & Rowlands, R (2002). Moiré-Numerical Hybrid Analysis of Cracks in Orthotropic Media, *Experimental Mechanics*, Vo.42, No.3, pp. 311-317, ISSN 1741-2765

Baek, T. & Rowlands, R. (2001). Hybrid Stress Analysis of Perforated Composites using Strain Gages, *Experimental Mechanics*, Vol.41, No.2, pp. 194-202, ISSN 1741-2765

Sanford, R. (1980). Application of the Least-Squares Method to Photoelastic Analysis, Experimental Mechanics, Vol.20, No.6, pp. 192-197, ISSN 1741-2765

Morimoto, Y. & Fujisawa, M. (1994). Fringe Pattern Analysis by a Phase-Shifting Method using Fourier Transform, *Optical Engineering*, Vol.33, No.11, pp. 3709-3714

Kim, M. ; Baek, T., Morimoto, Y., & Fujigaki, M. (2005). Application of Phase-shifting Method using Fourier Transform to Measurement of In-plane Displacement by Speckle Interferometry, *Journal of the Korean Society for Nondestructive Testing*, Vol.25, No.3, pp. 171-177

Baek, T.; Chung, T. & Panganiban, H. (2008). Full-Field Stress Determination Around Circular Discontinuity in a Tensile-Loaded Plate using x-displacements Only, *Journal of Solid Mechanics and Material Engineering*, Vol.2, No.6, pp. 756-762

Baek, T. & Rowlands, R. (1999). Experimental Determination of Stress Concentrations in Orthotropic Composites, *Journal of Strain Analysis*, Vol.34, No.2, pp. 69-81, ISSN 0309-3247

Baek, T. & Rudolphi, T. (2010). A Hybrid Stress Measurement Using only x-displacement by Phase Shifting Method with Fourier Transform (PSM/FT) in Laser Speckle Interferometry and Least Squares Method, *International Journal of Precision Engineering and Manufacturing*, Vol.11, No.1, Korean Society for Precision Engineering, pp. 49-54, ISSN 0217-9849

Interferometry - Research and Applications in Science and Technology

Edited by Dr Ivan Padron

ISBN 978-953-51-0403-2

Hard cover, 462 pages

Publisher InTech

Published online 21, March, 2012

Published in print edition March, 2012

This book provides the most recent studies on interferometry and its applications in science and technology. It is an outline of theoretical and experimental aspects of interferometry and their applications. The book is divided in two sections. The first one is an overview of different interferometry techniques and their general applications, while the second section is devoted to more specific interferometry applications comprising from interferometry for magnetic fusion plasmas to interferometry in wireless networks. The book is an excellent reference of current interferometry applications in science and technology. It offers the opportunity to increase our knowledge about interferometry and encourage researchers in development of new applications.

How to reference

In order to correctly reference this scholarly work, feel free to copy and paste the following:

INTECH

open science | open minds